

Mechanical Properties of Toughened $\text{Al}_2\text{O}_3\text{-ZrO}_2\text{-TiN}$ Ceramics

D. Ostrovoy,^a N. Orlovskaya,^b V. Kovylyaev^b and S. Firstov^b

^aThe Institute for Problems of Strength, National Academy of Sciences of Ukraine, 2 Timiryazevskaya St. 252014 Kiev-14, Ukraine

^bThe Institute for Problems of Materials Science, National Academy of Sciences of Ukraine, 3 Krzhizhanovskogo St. 252180 Kiev-180, Ukraine

(Received 10 February 1997; accepted 3 July 1997)

Abstract

Mechanical properties, phase composition and microstructure of ceramics in the system $\text{Al}_2\text{O}_3\text{-ZrO}_2\text{-TiN}$ (AZT) were studied on bending and indentation in the range of 20–1400°C. Small Y_2O_3 amounts added to stabilize ZrO_2 were established to result in higher strength of these materials at higher temperatures (up to 1000°C). The oxidation of TiN at 700°C and above induces the degradation of strength of AZT ceramics. Higher test temperatures lead to the change of microstructure and phase composition of an oxide layer and its resistance to indentation. At 1000 and 1200°C rutile and at 1400°C aluminum titanate and Ti_5O_9 are formed on the AZT surface. Titanium nitride present in AZT ceramics contributes to an increase in their fracture toughness as compared to the $\text{Al}_2\text{O}_3\text{-ZrO}_2$ ones. © 1998 Published by Elsevier Science Limited.

1 Introduction

The phase transformation in zirconia particles added to alumina-based ceramics enhances their mechanical properties enlarging the scope of their application (see for example Refs 1–5). However the strength and fracture toughness of such ceramics decrease with temperature.^{6–8} They start to undergo plastic deformation at 1000°C and above due to grain-boundary sliding of second-phase particles by superplasticity mechanism.^{7,9,10} The addition of titanium nitride particles to alumina is known to also improve the mechanical characteristics and to greatly influence the thermal stability of this two-phase material.¹¹

Advanced properties of an $\text{Al}_2\text{O}_3\text{-TiN}$ composite are associated with crack deflection and crack pinning mechanisms due to the presence of second-

phase particles.^{8,11,12} However, the titanium nitride oxidation at temperatures above 700°C can exert a negative influence on the strength of such materials and restrict their high-temperature performance.¹³

Fine-dispersed TiN particles added to $\text{Al}_2\text{O}_3\text{-ZrO}_2$ ceramics and uniformly distributed in their bulk contribute to higher strength at room and elevated temperatures.^{14–16} However, the effect of different compositions of $\text{Al}_2\text{O}_3\text{-ZrO}_2\text{-TiN}$ ceramics on the variation of their properties over a wide temperature range still remains insufficiently studied. It particularly refers to the investigation of their phase composition and their toughening mechanisms at different temperatures.

The present work is devoted to the studies on such mechanical properties as strength, hardness and fracture toughness of ceramics in the system $\text{Al}_2\text{O}_3\text{-ZrO}_2\text{-TiN}$ at various loading modes and temperatures. For comparison similar investigations were performed for ceramics in the system $\text{Al}_2\text{O}_3\text{-ZrO}_2$.

2 Materials and Methods

The $\text{Al}_2\text{O}_3\text{-ZrO}_2\text{-TiN}$ ceramics (AZT) possess the composition given in Table 1. As is seen in this Table, the amount of a ZrO_2 transformation toughening additive is changed in parallel with that of the Y_2O_3 stabilizing additive. The TiN content was 23 wt% providing an acceptable strength value (see also Ref. 11). Comparative tests were performed on the $\text{Al}_2\text{O}_3\text{-ZrO}_2$ ceramics (AZ) containing 30 wt% ZrO_2 (3 mol% Y_2O_3)^{14,17}. The materials were produced from $\alpha\text{-Al}_2\text{O}_3$, monoclinic (*m*) ZrO_2 , Y_2O_3 , and TiN powders with particle sizes of 2.5, 11.0, 10.0, and 5.5 μm , respectively (Laser Micron Sizer). The powders were mixed at a given ratio and ground in a ball mill to a particle

Table 1. Chemical composition of an AZT mixture (wt%)

Material	Al ₂ O ₃	ZrO ₂	Y ₂ O ₃	TiN
AZT-1	54.0	23.0	3.0 ^a	23.0
AZT-2	62.0	15.0	2.5 ^a	23.0
AZT-3	62.0	15.0	1.3 ^a	23.0

^amol% as ZrO₂.

size of 1.1 μm. Then they were hot-pressed in BN-lined graphite moulds at temperature of 1600°C and pressure of 25 MPa for 1 h. The specimens were of dark-golden colour for AZT and of dark-grey colour for AZ.

Mechanical tests were carried out in several stages. First, the bending strength (σ_f), maximum strain at the moment of specimen fracture (ε_f), and static elastic modulus (E_{st}) were determined by a procedure.¹⁸ Prismatic specimens with a 3.5 × 5.0 mm² cross-section were loaded on three- and four-point bending in air at 20–1000°C (several specimens were heated up to 1400°C). In the first case the test span was 20 mm, in the second case the inner and outer spans were 20 and 40 mm, respectively. Before bending tests the specimens were kept in the furnace for 0.5 h at preset temperature. The cross-head speed was 0.5 mm min⁻¹.

The values of mechanical characteristics were calculated by known equations of applied mechanics:

$$\sigma_f = \frac{3fP}{bh^2}, \quad \varepsilon_f = \frac{kh\delta}{L^2}, \quad E_{st} = \left(\frac{d\sigma}{d\varepsilon} \right)_{\varepsilon \rightarrow 0}, \quad (1)$$

where P is the load; δ is the specimen deflection; f is the cantilever part of the specimen; L is the span on three-point bending ($k = 6$) and the inner span on four-point bending ($k = 4$); b and h are the width and height of the specimen, respectively. The value of E_{st} was estimated by the slope of the initial portion of the load (P) versus deflection (δ) curve at the origin of co-ordinates.¹⁸

Fracture toughness (K_{Ic}) was measured on three-point bending of the SENB specimens (notch width ≈ 150 μm). The calculations were performed by the equation: $K_{Ic} = \sigma_f \alpha^{0.5} Y$, where (α) is the length of the notch; $Y = f[(\alpha/h)]$ is the geometric factor.¹⁹ The cross-head speed was 0.1 mm min⁻¹.

The second stage of mechanical tests included the determination of hardness (H_v) and fracture toughness (K_{cv}) on the Vickers indentation. A part of specimens after bending tests were polished with diamond pastes and then indented. Hardness was calculated by the equation: $H_v = 463.6P/a^2$, where P is the load in N, a is the half-diagonal of the indenter impression in μm.²⁰ The equations for the K_{cv} calculation are given below.

The microstructure of specimens before and after high-temperature testing was studied by scanning

electron microscopy (SEM). The phase composition of ceramics was analyzed by X-ray diffraction (XRD) (DRON-4M, Cu K α radiation).

3 Results and Discussion

3.1 Bending tests

The results of preliminary tests of AZT-1, AZT-2, and AZT-3 specimens demonstrate [Fig. 1(a)] that the amount of ZrO₂ and Y₂O₃ influences the strength, σ_f , in the range of 20–1000°C. Differences in σ_f values are also observed at room temperature which is associated with a varying phase composition of zirconia (see also Ref. 14).

At higher temperatures the differences in strength of the materials under study are growing. Strength (σ_f) versus temperature (T) curves exhibit a typical run over different temperature ranges [Fig. 1(a)]. It should be noted that the maximum on the σ_f versus T curve is dependent on Y₂O₃ contents in ZrO₂; it is shifted to higher temperatures with a smaller amount of yttria. It can be explained by the fact that a smaller amount of Y₂O₃ results in the shift of temperature of the $t \rightarrow m$ transition in ZrO₂ to higher values.²¹ Thus, when the test temperature coincides with the temperature of martensite transformation in ZrO₂, σ_f increases, since higher temperature stabilizes a high-temperature tetragonal phase and the load applied induces the $t \rightarrow m$ transformation, therefore the initiation of $t \rightarrow m$ requires higher critical stresses.

To establish a temperature dependence of strength in more detail, AZT-1 specimens were chosen for four-point bending test, i.e. they were under linear stress conditions unlike plane stress ones occurring in the specimens on three-point bending. The temperature dependencies [Fig. 1(b)] of major mechanical characteristics of AZT-1, namely σ_f , ε_f , and E_{st} , can indirectly point to different toughening mechanisms appearing in such material with temperature variations.

From the qualitative point of view, the K_{Ic} versus T curve [Fig. 1(a)] practically repeats a similar curve for σ_f . It can be explained by the shape of a stress concentrator in the SENB specimens which is a notch with a fixed radius of curvature (~ 75 μm) at its tip as opposed to a 'sharp' crack.²²

The temperature range of testing can be divided into several subranges within which different toughening mechanisms can exist.

At room temperature and temperatures close to it mechanical properties (strength and fracture toughness) of AZT-1 are most likely controlled by several mechanisms: (i) stress-induced transformation toughening due to t -ZrO₂ particles (also typical of AZ ceramics); (ii) microcracking toughening,

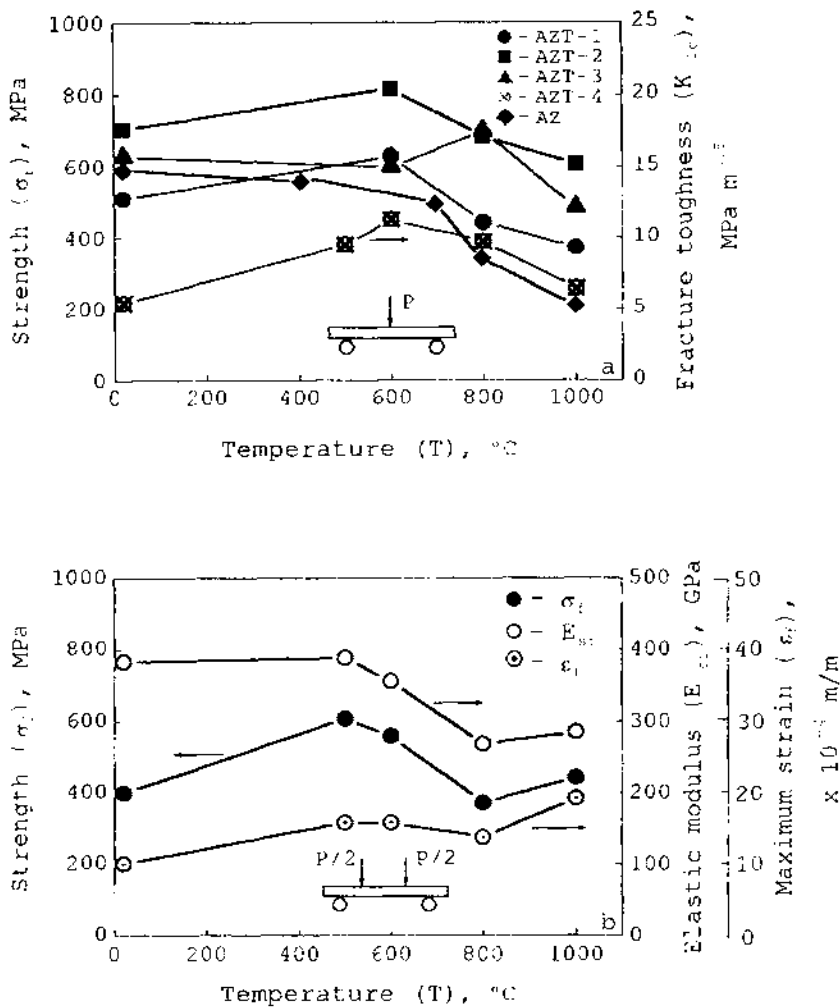


Fig. 1. Temperature dependences of mechanical characteristics of AZT on (a) three- and (b) four-point bending: ●, ■, ▲, ◆, ⊗, ⊙ - K_{Ic} ; ○, ⊙ - E_{sf} ; ○, ⊙ - ϵ_f ; ◆ - AZ.

since ceramics contained a small amount of monoclinic zirconia formed as a result of cooling of ceramics after hot pressing, (iii) crack deflection toughening associated with the distribution of finely dispersed TiN particles in the bulk of the material.^{1,2,4,5,8,12,14}

At 500–600°C one can observe strength [Fig. 1(b)] and fracture toughness [Fig. 1(a)] maxima which can be related both to the transformation toughening (induced by stress and/or temperature) and to the dispersion toughening. With a further increase in temperature the effect of transformation toughening in AZT-1 gradually decreases, while relaxation processes are activated which result in a lower E_{sf} value [Fig. 1(b)].⁸ At 900–1000°C load versus deflection curves begin deviating from linearity, ϵ_f starts growing, an inconsiderable local increase of σ_f takes place [Fig. 1(b)]. It can be explained by reaching so-called brittle-to-ductile transition temperature, T_{BD} , above which creep and subcritical crack growth start noticeably activating.^{2,1,24} These processes lead to a considerable strength loss of AZT-1

above 1000°C (not shown in Fig. 1) and its practical application becomes problematic. The mechanism which can retard the deterioration of mechanical properties of AZT-1 is most likely dispersion toughening. The TiN particles possess rather high melting temperature (2950°C) which allows to deviate or even arrest cracks in the material, especially when this process occurs on grain boundaries as a result of softening the boundary phase at reaching or exceeding the temperature T_{BD} .^{8,11,12,25} In AZ the degradation of strength [Fig. 1(a)] starts increasing at comparatively low temperatures (800–850°C) because the above toughening mechanism is absent.

Above 600–700°C titanium nitride starts oxidizing.^{11,13,26} With this the specimen surfaces are covered with a bright layer of titanium oxides the thickness and colour of which increases and changes with test temperature and time the specimens kept at preset temperature. Such layer contains a great number of pores and other defects (see also Refs 11, 26). Therefore lower strength of AZT-1 above 600°C can additionally be associated with

the TiN oxidation. The strength of AZT-1 at room temperature decreases after preannealing of specimens at 1000–1400°C in air which could also be associated both with the oxidation and with the destroying of the transformation zone in the specimens.^{8,27}

The phase composition of AZT-1 surfaces at different temperatures is given in Fig. 2. At room temperature they contained α -Al₂O₃, *m*-, *t*-, *c*-ZrO₂, and TiN. The *c*-ZrO₂ is not shown in this figure because of its ill-pronounced X-ray reflections. As a result of oxidation, rutile, TiO₂, was formed at 1000°C. When temperature increases up to 1200°C, its quantity on the specimen surface increases considerably, at the same time the quantity of titanium nitride decreases. It should be noted that the oxidation at 1200°C results in a thicker oxide layer, therefore the intensity of alumina and zirconia maxima greatly decreases. At 1400°C rutile was not revealed, and as a result of diffusion processes, titanium suboxide, Ti₅O₉, and aluminum titanate, Al₂TiO₅, were formed. These data are in good agreement with the fact that the number of metal particles in an oxide layer increases with temperature and their transformation into suboxides proceeds more rapidly.²⁸ It is associated with substitution of oxygen for nitrogen which

results in the release of metal into the surface layer. The release of metal and nonmetal during titanium nitride oxidation in AZT-1 determined by the formation of vacancies in both sublattices of oxynitride solid solutions exerts a considerable influence on mechanical characteristics of oxidized AZT-1 specimens.²⁸

At 1200°C an oxide layer is tightly cohered with the specimen surface. At 1400°C the thickness of an oxide layer increased considerably, it consisted of several sublayers having different microstructure (Fig. 3). The relief of the oxide layer exhibited quite developed (rough) fracture surface which was not observed after tests of the specimens at room temperature as well as at 1000°C and 1200°C. The main crack which fractures the specimens primarily propagated through this layer in an intercrystallite mode with noticeable branching and grain separation [Fig. 3(c) and (d)]. The fracture in the centre of the specimen cross-section was characterized by both the transcrystallite and intercrystallite steps [Fig. 3(e)] as observed at lower temperatures. Intensive gas evolution gave rise to pores and microflaws on the material-oxide layer interface, these cause the separation of this layer from the composite in several places [Fig. 3(f)].

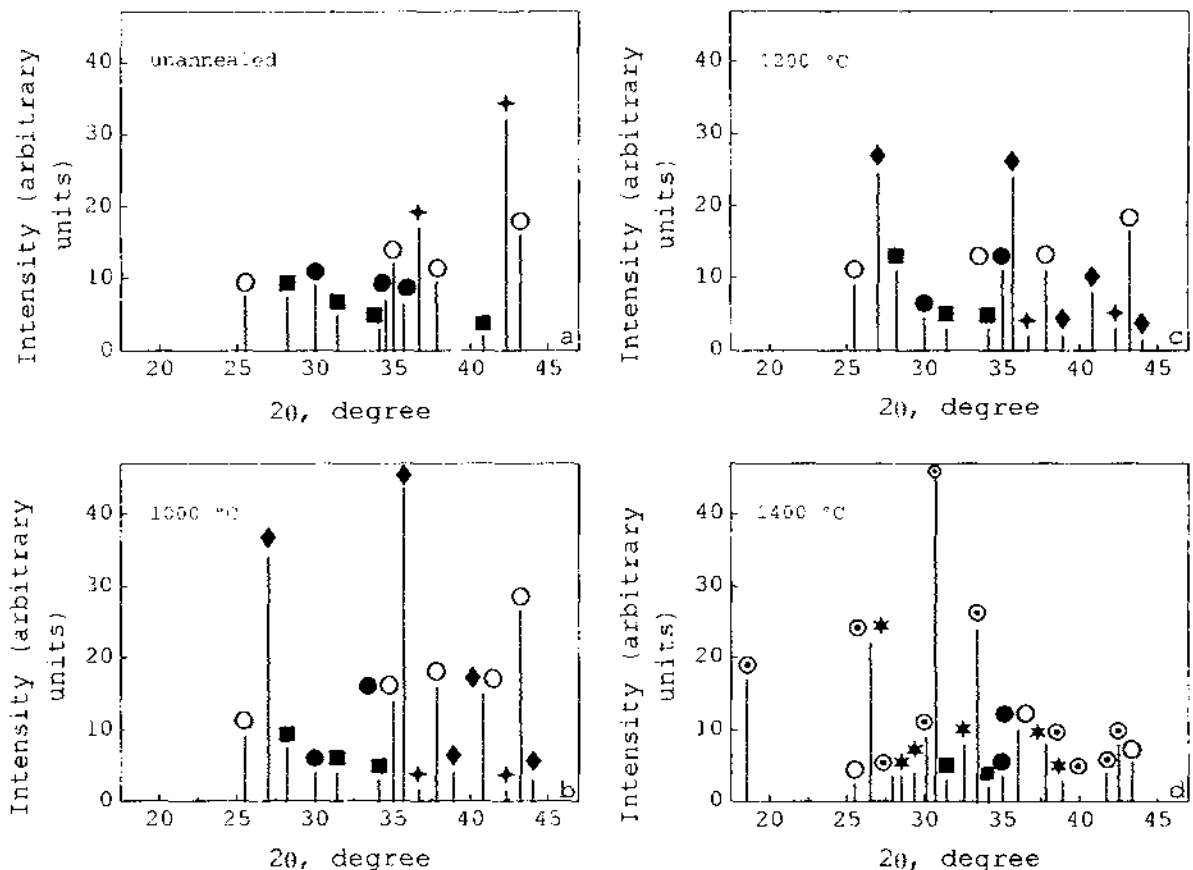


Fig. 2. XRD results for AZT-1 (a) before and (b–d) after high-temperature tests: ○ α -Al₂O₃, ■ *m*-ZrO₂, ● *t*-ZrO₂, ♦ TiN, * Ti₅O₉, ⊙ Al₂TiO₅, ◆ TiO₂.

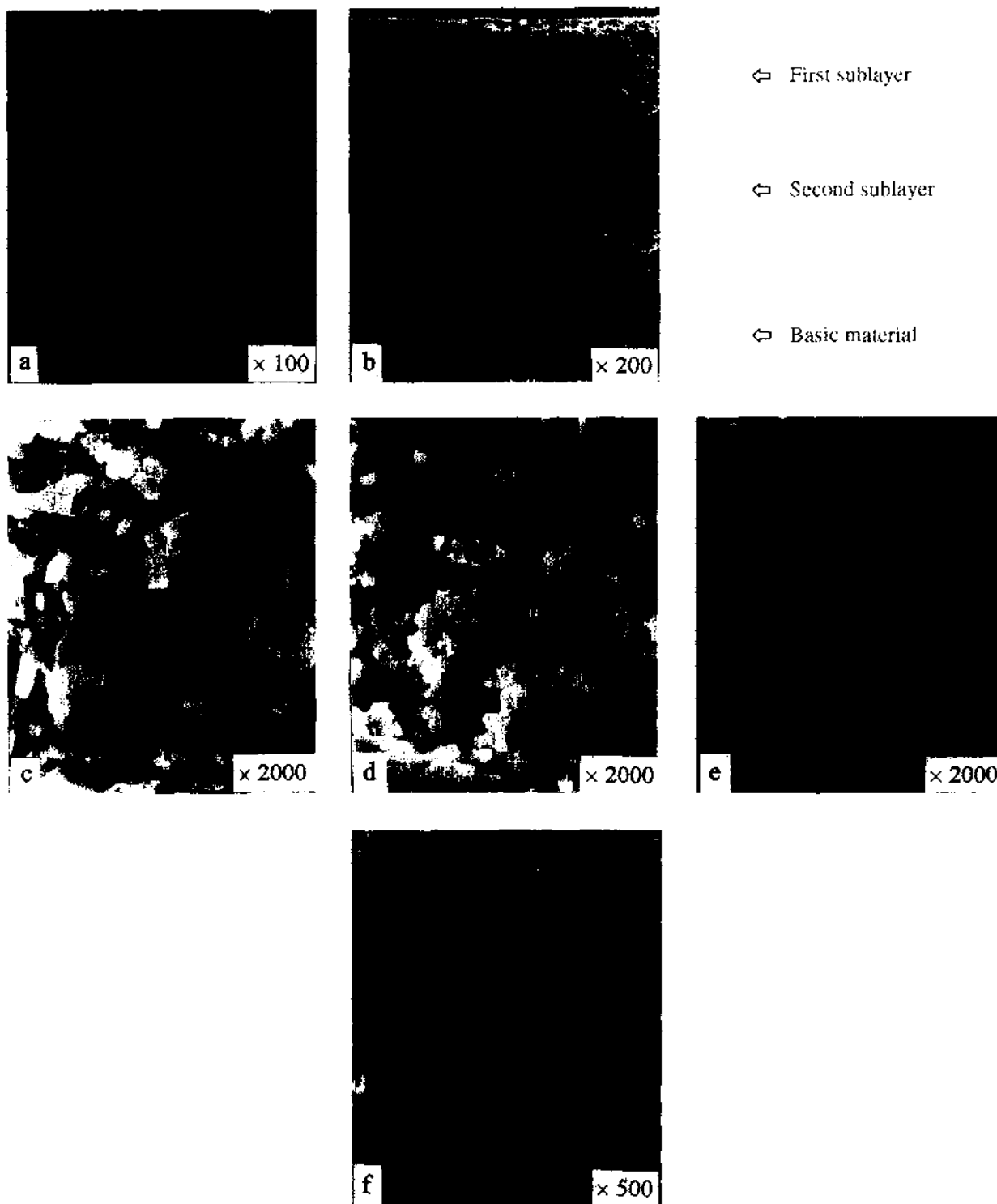


Fig. 3. SEM micrographs of the surfaces of an AZT-1 specimen tested at 1400°C: view of the part of a fracture surface (a); oxide sublayers (b); main crack propagation through the first (c) and second (d) sublayers and the centre of the specimen (e); separation of an oxide layer from the basic material (f).

3.2 Indentation tests

3.2.1 Hardness

Hardness, H_v , was studied at room temperature on AZT-1 and AZ specimens both in the initial state (after machining) and after testing at 1000, 1200, and 1400°C.

AZT-1 as well as AZ in their initial state are characterized by a descending Vickers hardness

(H_v) versus applied load (P) relationship (scattered plot in Fig. 4). Such dependence is often observed for other ceramic materials which can particularly be explained by the extent of damage of the surface layer on machining, by the formation of cracks around indenter impressions, etc.²⁰ The values of H_v were 15–17 GPa in the present work, while higher values of 21–22 GPa were cited in.¹⁶ It is noteworthy that the value of H_v does not

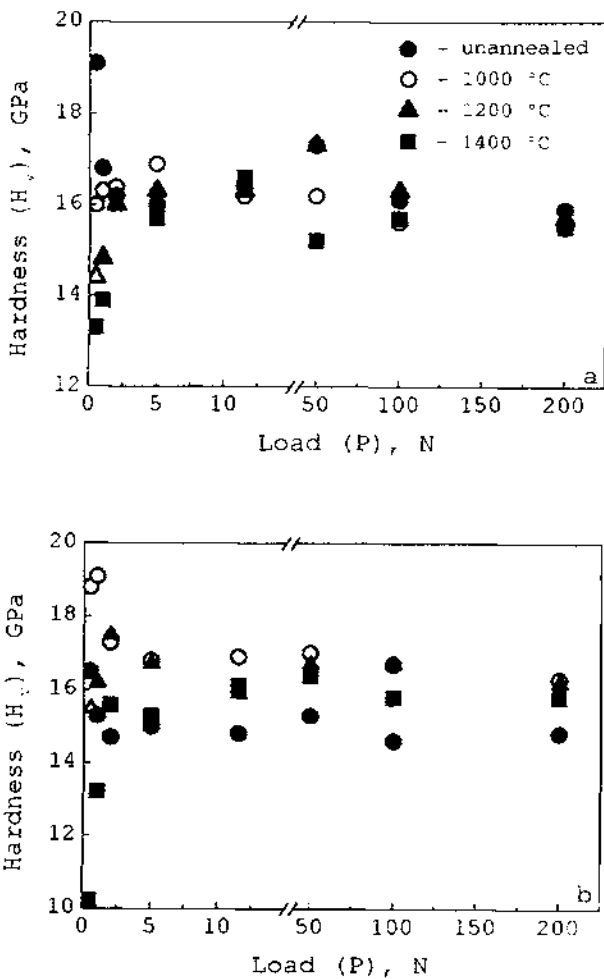


Fig. 4. Hardness (H_v) versus applied load (P) for (a) AZ and (b) AZT-1 at room temperature after high-temperature tests.

practically depend on the load applied (Fig. 4) from the moment when first cracks appear around the impressions.

The effect of test temperature on room-temperature hardness is of somewhat contradictory nature. Thus, after tests at 1000°C the hardness versus load plot for AZT-1 as well as for initial specimens was descending [Fig. 4(b)]. For AZ this dependence was rather ill-pronounced [Fig. 4(a)]. The tests at 1200 and 1400°C result in ascending portions (Fig. 4) of the above plot at small loads (less than 5 N), these portions being more pronounced for the specimens heated up to 1400°C. Such effects on H_v can most likely be related to the surface layer formed on oxidation of AZT-1 (Fig. 3) and AZ.¹⁷ A considerable scatter of experimental values of H_v for AZT-1 can be associated with higher oxidability of the material on heating and, as a result, more extensive stress corrosion, composition heterogeneity and nonuniformity in defect distributions. The oxidation of titanium nitride and the formation of titanium-containing oxide phases are accompanied by the release of titanium and nitrogen from the titanium

nitride lattice and their diffusion into the oxide layer. At relatively low temperatures (1000 and 1200°C) XRD demonstrates (Fig. 2) a lower intensity of peaks of α - Al_2O_3 lines which points to a thicker rutile layer on the surface and to the absence of diffusion or even inconsiderable diffusion of $\text{Al}^{(3+)}$ atoms (ions) onto the surface. At 1400°C the $\text{Al}^{(3+)}$ diffusion is activated which leads to the formation of flaky aluminum titanate grains. These processes can determine the variation of phase composition and microstructure of the oxide layer, and, thus, its microhardness.

3.2.2 Fracture toughness

The indentation tests of AZT-1 and AZ specimens demonstrated that the load values at which radial cracks appeared from the corners of the indenter impressions were about 5 N for both materials. However, for AZT-1 such cracks from all the four corners of Vickers impressions were observed starting from a load of 50 N. For AZ it was equal to 11.5 N. In other words, these preliminary data are indicative of higher fracture toughness of AZT-1 as compared to AZ.

To quantitatively evaluate the fracture toughness, radial crack length (c) versus impression half-diagonal (a) curves were plotted (Fig. 5). It should be noted that the length of radial cracks near the impressions was measured with the account of their half-diagonals, as it is usually done in practice, e.g.²⁰ These relations for AZT-1 and AZ are described by the following equations:

$$c = 0.42a^{1.42} \tag{2}$$

$$c = 0.88a^{1.3} \tag{3}$$

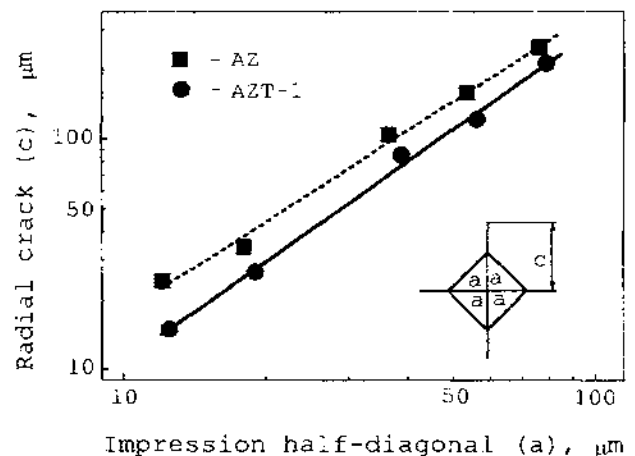


Fig. 5. Length of radial cracks (c) versus applied load (P) for AZ and AZT-1 ceramics at room temperature.

Table 2. The equations for K_{Ic} , determining from Vickers indentations^a

Equation	Crack type	Reference
a. $(0.129H_v a^{0.5}/\phi)(E\phi/H_v)^{0.4}(c/a)^{1.5}$	Median crack	29
b. $(0.035H_v a^{0.5}/\phi)(E\phi/H_v)^{0.4}(c/a)^{0.5}$	Radial (Palmqvist) crack	29
c. $(0.142H_v a^{0.5}/\phi)(E\phi/H_v)^{0.4}(c/a)^{1.56}$	Median + radial (Palmqvist) crack (curve-fitting method)	30
d. $(0.099H_v a^{0.5}/\phi)(E\phi/H_v)^{0.4}(c/a)^{1.48}$	Curve-fitting method	Present work
e. $(0.070H_v a^{0.5}/\phi)(E\phi/H_v)^{0.4}(c/a)^{1.11}$	Curve-fitting method	Present work

^a H_v is the Vickers hardness; E is the elastic modulus; ϕ is the constraint factor ($\phi \approx 3$); P is the load on the indenter; a and c are as shown in Fig. 5.

The influence of test temperature on the length of such cracks was of rather contradictory nature which was associated with the formation of an oxide layer and its heterogeneity for different specimens. Therefore surface fracture toughness was evaluated only on the specimens which were not thermally treated. For this purpose known equations, e.g. (a)–(c) (Table 2) were first used to determine the value of stress intensity factor, K_{Ic} , on Vickers indentation.

K_{Ic} obtained from these equations exhibits rather wide scatter of values (Fig. 6). The values of stress intensity factor obtained by different methods were

cited earlier, they are within 4.5–6.0 MPa m^{0.5} on the average.^{14,16} The bending of SENB specimens gave $K_{Ic} = 5.58$ and 3.83 MPa m^{0.5} for AZT-1 and AZ, respectively. The authors used an approach of setting the accordance with stress intensity factor values obtained by indentation and bending.^{31,32} For this purpose the calibration curves for AZT-1 and AZ were plotted being normalized fracture toughness $[(K_{Ic}\phi/H_v a^{0.5})(H_v/E\phi)^{0.4}]$ versus normalized radial crack length (c/a) relations (Fig. 7). These curves were obtained proceeding from $K_{Ic} = K_{Ic}$ values determined by the SENB method. The method of least squares was used to derive equations (d) and (e) in Table 2 for evaluating the fracture toughness of AZ and AZT-1, respectively. The K_{Ic} values calculated by these equations are practically independent of the load and are in good agreement with the K_{Ic} data (Fig. 6). The difference in numerical coefficients in the equations derived and in eqns (a)–(c) (see Table 2) is most likely associated with different crack propagation patterns in the ceramics under study as compared to other materials for which eqns (a)–(c) were obtained.

The results (Fig. 6) have demonstrated once more that the TiN addition to Al₂O₃-ZrO₂ ceramics increases their fracture toughness.

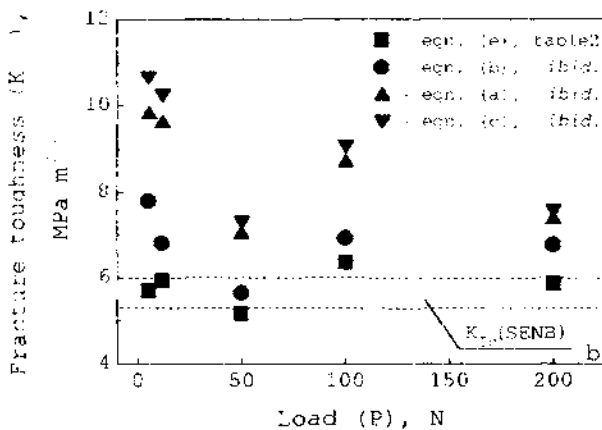
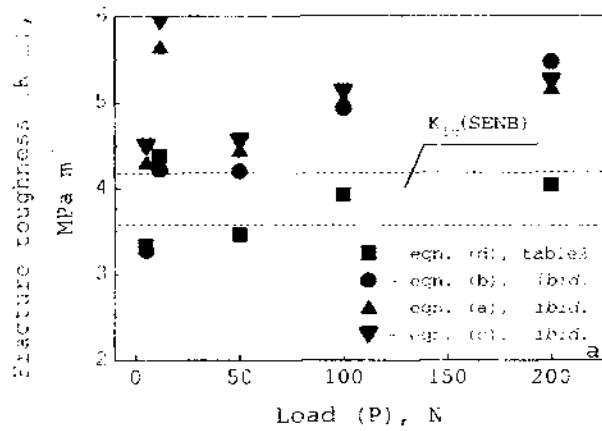


Fig. 6. Indentation fracture toughness (K_{Ic}) versus applied load (P) for (a) AZ and (b) AZT-1 ceramics at room temperature.

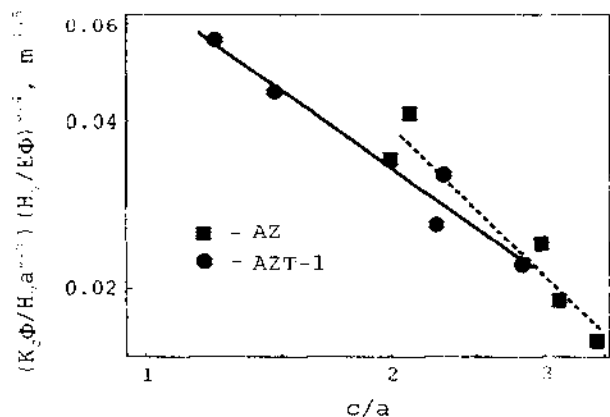


Fig. 7. Normalized fracture toughness $[(K_{Ic}\phi/H_v a^{0.5})(H_v/E\phi)^{0.4}]$ versus normalized radial crack length (c/a) for AZ and AZT-1 ceramics at room temperature.

4 Conclusions

The results for $\text{Al}_2\text{O}_3\text{-ZrO}_2\text{-TiN}$ composites can lead to the following conclusions: (i) material containing ZrO_2 with a lower Y_2O_3 amount possesses higher strength at higher temperatures; (ii) strength degradation can additionally occur due to the TiN oxidation above 700°C ; (iii) higher test temperatures cause a greater thickness of an oxide layer and variation of its phase composition and colour (at 1000 and 1200°C it consists of titania as rutile, at 1400°C aluminum titanate and Ti_5O_9 are formed); (iv) hardness of an oxide layer depends on its microstructure and phase composition determined by temperature conditions; (v) TiN addition to $\text{Al}_2\text{O}_3\text{-ZrO}_2$ ceramics increases their fracture toughness.

Acknowledgements

The authors are pleased to acknowledge the support of the State Committee for Science and Technology of Ukraine. This work was also supported, in part, by a Soros Humanitarian Foundations Grant awarded by the American Physical Society.

References

1. Claussen, N., Fracture toughness of Al_2O_3 with an unstabilized ZrO_2 dispersed phase. *J. Am. Ceram. Soc.*, 1976, **59**, 49–51.
2. Lange, F. F., Transformation toughening: Part 4. Fabrication, fracture toughness and strength of $\text{Al}_2\text{O}_3\text{-ZrO}_2$ composite. *J. Mater. Sci.*, 1982, **17**, 247–254.
3. Becher, P. F. and Tennery, V. J., Fracture toughness of $\text{Al}_2\text{O}_3\text{-ZrO}_2$ composites. In *Fracture Mechanics of Ceramics*, Vol. 6, eds R. C. Bradt, A. G. Evans, D. P. H. Hasselman and F. Lange. Plenum, New York, 1983, pp. 383–399.
4. Wang, G. and Stevens, R., Zirconia-toughened alumina (ZTA) ceramics. Review. *J. Mater. Sci.*, 1989, **24**, 3421–3440.
5. Karihaloo, B. L., Contribution of $t \rightarrow m$ phase transformation to the toughening of ZTA. *J. Am. Ceram. Soc.*, 1991, **74**, 1703–1706.
6. Fukuhara, M., Properties of $[\text{Y}] \text{ZrO}_2\text{-Al}_2\text{O}_3\text{-}[\text{Y}] \text{ZrO}_2\text{-Al}_2\text{O}_3\text{-}[\text{Ti or Si}] \text{C}$ composites. *J. Am. Ceram. Soc.*, 1989, **72**, 236–242.
7. Krell, A., Riech, T., Beger, A., Gogotsi, G. A. and Groushevsky, Y. L., The effect of SiO_2 on high-temperature deformation and strength of zirconia-toughened alumina. *J. Mater. Sci.*, 1991, **26**, 4637–4642.
8. Faber, K. T., Toughening mechanisms for ceramics in automotive applications. *Ceram. Eng. Sci. Proc.*, 1984, **6**, 408–439.
9. Calderon-Moreno, J. M., De Arellano-Lopez, A. R., Dominguez-Rodriguez, A. and Routbort, J. L., Microstructure and creep properties of alumina/zirconia ceramics. *J. Eur. Ceram. Soc.*, 1995, **15**, 983–988.
10. Wakai, F., Kato, H. and Sakaguchi, S. et al., Compressive deformation of Y_2O_3 -stabilized $\text{ZrO}_2\text{-Al}_2\text{O}_3$ composite. *J. Ceram. Soc. Jpn. (Yogyo-Kyokai-Shi)*, 1986, **94**, 1017–1020.
11. Bellosi, A., Portu, G. and Guicciardi, S., Preparation and properties of electroconductive Al_2O_3 -based composites. *J. Eur. Ceram. Soc.*, 1992, **10**, 307–315.
12. Evans, A. G., Perspective of the development of high toughness ceramics. *J. Am. Ceram. Soc.*, 1990, **73**, 187–206.
13. Tampieri, A., Landi, E. and Bellosi, A., The oxidation behaviour of monolithic TiN Ceramics. *Br. Ceram. Trans. J.*, 1991, **90**, 194–196.
14. Gogotsi, Y. G., Grigoriyev, O. N., Orlovskaya, N. A., Ostrovoy, D. Y. and Yaroshenko, V. P., Strengthened Al_2O_3 -based ceramics. *Refractories*, 1989, **30**, 667–670 (Transl. from Russian).
15. Grigoriyev, O. N., Gogotsi, Y. G., Orlovskaya, N. A. and Khomenko, G. E., Effect of TiN on the mechanical properties of $\text{Al}_2\text{O}_3\text{-ZrO}_2$ ceramics. In *Proceedings of Second Euro-Ceramics*, ed. G. Ziegler and H. Hausner. Deutsche Keramische Gesellschaft e. v., Augsburg, 1991, pp. 1413–1417.
16. Rak, Z. S. and Van Tilborg, P. J., Effect of TiN and SiC on the mechanical properties of ZTA ceramics. In *Proceedings of Third Euro-Ceramics*, ed. P. Duran and J. F. Fernandez. Faenza Editrice Iberica S. L., Faenza, 1993, pp. 767–772.
17. Orlovskaya, N., Krivoshej, G., Babij, O. and Ostrovoy, D., Effect of annealing on microstructure, phase composition and failure of $\text{Al}_2\text{O}_3\text{-ZrO}_2$ ceramics at room temperature. *J. Mater. Sci. Lett.*, 1996, **15**, 166–169.
18. Gogotsi, G. A. and Ostrovoy, D. Yu., Deformation and strength of engineering ceramics and single crystals. *J. Eur. Ceram. Soc.*, 1995, **15**, 271–281.
19. Brown, W. and Srawley, J. E., *Plane strain crack toughness testing of high strength metallic materials*. ASTM STP 410. *Am. Soc. Test. Mater.*, 1966, pp. 1–129.
20. Li, Z., Ghosh, A., Kobayashi, A. S. and Bradt, R. C., Indentation fracture toughness of sintered silicon carbide in the Palmqvist crack regime. *J. Am. Ceram. Soc.*, 1989, **72**, 904–911.
21. Orlovskaya, N. A., Development of hot-pressed alumina-based composite ceramics with high physico-mechanical properties for structural and tool applications. Ph.D. thesis. The Institute for Problems of Materials Science, Ukraine, Kiev, 1993.
22. Wang, J., Rainforth, W. M., Wadsworth, I. and Stevens, R., The effect of notch width on the SENB toughness for oxide ceramics. *J. Eur. Ceram. Soc.*, 1992, **10**, 21–31.
23. Evans, A. G. and Dalgleish, B. J., Some aspects of the high temperature performance of ceramics and ceramics composites. *Ceram. Eng. Sci. Proc.*, 1986, **7**, 1073–1094.
24. Sato, K., Tanaka, K., Nakano, Y. and Mori, T., Temperature dependence of anelastic deformation in polycrystalline silicon nitride. *J. Am. Ceram. Soc.*, 1993, **76**, 2042–2048.
25. Andriyevsky, R. A., Lanin, A. G. and Rimashevsky, G. A., *Strength of high-melting compounds*. Metallurgy, Moscow, 1974, p. 12.
26. Gogotsi, Y. G., Porz, F. and Yaroshenko, V. P., Mechanical properties and oxidation behavior of $\text{Al}_2\text{O}_3\text{-AlN-TiN}$ composites. *J. Am. Ceram. Soc.*, 1992, **75**, 2251–2259.
27. Swain, M. V. and Claussen, N., Comparison of K_{Ic} values for $\text{Al}_2\text{O}_3\text{-ZrO}_2$ composites obtained from notched-beam and indentation strength techniques. *J. Am. Ceram. Soc.*, 1983, **66**, C-27–C-29.
28. Voytovich, R. F., *Oxidation of Carbides and Nitrides*. Naukova Dumka, Kiev, 1981, p. 192.
29. Niihara, K., Morena, R. and Hasselman, D. P. H., Evaluation of K_{Ic} of brittle solids by the indentation method with low crack-to-indenter ratios. *J. Mater. Sci. Lett.*, 1982, **1**, 6–13.
30. Lankford, J., Indentation microcrack in the Palmqvist crack regime: implications for fracture toughness evaluation by the indentation method. *J. Mater. Sci. Lett.*, 1982, **1**, 493–495.
31. Evans, A. G. and Charles, E. A., Fracture toughness determinations by indentation. *J. Am. Ceram. Soc.*, 1976, **59**, 371–372.
32. Evans, A. G., ASTM STP 678. In *Fracture Mechanics Applied to Brittle Materials*. Am. Soc. Test. Mater., 1979, 112–135.